ELSEVIER

International Journal of Mass Spectrometry 177 (1998) 31–45

International Journal of Mass Spectrometry

Density functional study of mixed silicon carbide cluster cations $C_nSi_p^+$ ($n + p = 5,6$)

G. Pascoli[a,*], H. Lavendy[b]

[a]*Faculté des Sciences, Département de Physique, 33 rue Saint Leu Amiens 80039 Cedex, France*
[b]*Laboratoire de Dynamique Moléculaire et Photonique, CNRS (URA 779), Centre d'Etudes et de Recherches Lasers et Applications, Université de Lille1, Bat P5, 59655 Villeneuve d'Ascq Cedex, France*

Received 29 October 1997; accepted 23 January 1998

Abstract

The geometries and energies of the small silicon carbide cluster cations $C_nSi_p^+$ ($n + p = 5,6$) were investigated in a systematic manner by employing a functional density method. Several geometrical arrangements were considered for each cluster. Calculations always find a linear structure for these clusters when p (number of silicon atoms present in the structure) is smaller than n (number of carbon atoms). Conversely, for $p = n$ ($C_3Si_3^+$) or $p = n + 1$ ($C_2Si_3^+$), the structures appear planar in the ground state, and for $p > n + 1$, the three-dimensional forms become clearly favored. A comparison with the corresponding neutral isomers for $n + p = 6$, however, indicates that the emergence of the three-dimensionality is delayed for the cation with respect to the neutral species when proceeding from carbon-rich ($n > p$) to silicon-rich clusters ($n < p$). (Int J Mass Spectrom 177 (1998) 31–45) © 1998 Elsevier Science B.V.

Keywords: Carbon clusters; Cations; Silicon; Carbon; Silicone carbide; Mass spectrometry; Density functional theory

1. Introduction

Silicon-carbon clusters have been of significant interest in the past few years since the detection of spectral features of SiC, SiC_2, SiC_4 in circumstellar and interstellar environments [1,2]. Other larger clusters are very likely to also exist under various astrophysical conditions, as demonstrated by the presence of silicon carbide grains or microcrystals in meteorites [3]. Space, with its various conditions of density and temperature, constitutes a real laboratory to understand the mechanism of nucleation of both small clusters and grains of SiC. From a theoretical point of view, recent ab initio calculations are essentially focusing on neutral mixed silicon-carbon cluster systems [4–13]. In addition, in the laboratory, there exist a number of well-known experimental procedures (spark source mass spectrometry [14], secondary ion emission mass spectrometry [15], laser microprobe mass analysis, [16], and so on) for producing silicon-carbon clusters. In some variations of these mass spectrometric techniques, the clusters are observed as ionic species, such as perhaps, in the interstellar medium where carbon, with its relatively low ionization energy ~11 eV, is easily ionized by UV radiation of OB star associations. Hence, it is of interest to undertake a systematic study of the monopositive ions of silicon-carbon clusters. Small SiC cations $C_nSi_p^+$ ($n + p = 3,4$) have been theoretically investigated [17–19], while some of these, like $Si_2C_2^+$, were recently

* Corresponding author.

PII S1387-3806(98)14007-1

produced by laser vaporization of pellets made from a mixture of silicon and graphite powder [20,21].

The objective of the present study is to provide a comprehensive survey of the potential energy surface of larger mixed silicon-carbon cluster cations made of five or six atoms, with emphasis on the build-up mechanism and the nature of chemical bonding in these cations.

Sections 3 and 4 of this report are devoted to a detailed discussion on the geometries and electronic states considered for the individual clusters. We were interested in calculating a set of equilibrium geometrical parameters for the lowest nonplanar, rhomboidal, T-shaped, and linear isomers of each cluster, as well as their relative stabilities. For all related systems, except in a few cases, the lowest states have doublet multiplicities, quadruplets and sextuplets appear energetically above the corresponding doublet states. In section 5, we analyze the general aspects of the computed geometries and focus on the comparison between the structures and stability of low-lying geometries.

2. Computational details

All calculations were performed using the density functional method (DFT). The B3LYP exchange-correlation functional [22,23] has been used throughout this work. This consists of the Lee-Yang-Parr [24] correlation functional in conjunction with a hybrid exchange functional first proposed by Becke [25]. The latter is a linear combination of local density approximation, Becke's gradient correction [26], and the Hartree-Fock exchange energy based on Kohn-Sham [27] orbitals.

All calculations have been made using Pople's 6-311G* basis set [28] for carbon and silicon. As known, in density functional calculations such a basis set is able to give accurate results. Optimizations of geometries have been carried out with the GAUSSIAN94 package [29] running on an IBM RS/6000 and CRAY C98 at the National Computer Center Idris in Orsay (France). Each equilibrium geometry was characterized by analysis of the harmonic vibrational frequencies, obtained from analytic second-order derivative techniques. Local minima on the potential energy surface have no imaginary frequencies and saddle points do have one. Atomic charges, dipole moments, and rotational constants are also given.

3. Penta-atomic silicon-carbon clusters

The equilibrium geometries obtained for the low-energy $C_nSi_p^+$ $(n + p = 5)$ isomers are given in Fig. 1; bond lengths and bond angles and Mulliken atomic charges are also indicated. The electronic states, valence orbital configurations, energies, and dipole moments are listed in Table 1. The vibrational frequencies and zero-point energy corrections for these compounds are given in Table 2. In Table 3, the rotational constants of the ground state isomers are given.

3.1. C_5^+

The lowest electronic state of C_5^+ is found to be the linear $^2\Sigma_u^+$ (structure I, $D\infty h$). The electronic configuration is $\ldots(\pi_u)^4(\sigma_g)^2(\sigma_u)^1(\pi_g)^4$. With respect to the neutral C_5, the electron that is removed on ionization comes from a σ orbital and not a π orbital. The bond distances are 1.265 and 1.285 Å, similar to those of C_5 [30] and consistent with a cumulenelike structure. The distribution of charge is symmetrical and the median carbon is strongly positively charged $(0.68e)$. The monocyclic ring $^2A_1$ (structure II, C_{2v}) lies well above the ground state, at 95 kcal $\cdot$ mol^{-1}. Vibrational analysis indicates that this state is a saddle point on the potential energy surface and not a local minimum (three imaginary frequencies).

3.2. C_4Si^+

The ground state of C_4Si^+ is found to be the linear $^2\Sigma^+$ (structure III, $C_{\infty v}$). The silicon atom is in a terminal position in the cluster and bears the positive charge $(0.89e)$. The charge strongly oscillates along the carbon chain. The Si-capped bicyclic C_4 rhombus (structure IV, C_{2v}) is located at 46 kcal $\cdot$ mol^{-1} above the linear. This structure is a saddle point on the potential energy surface with one imaginary fre-

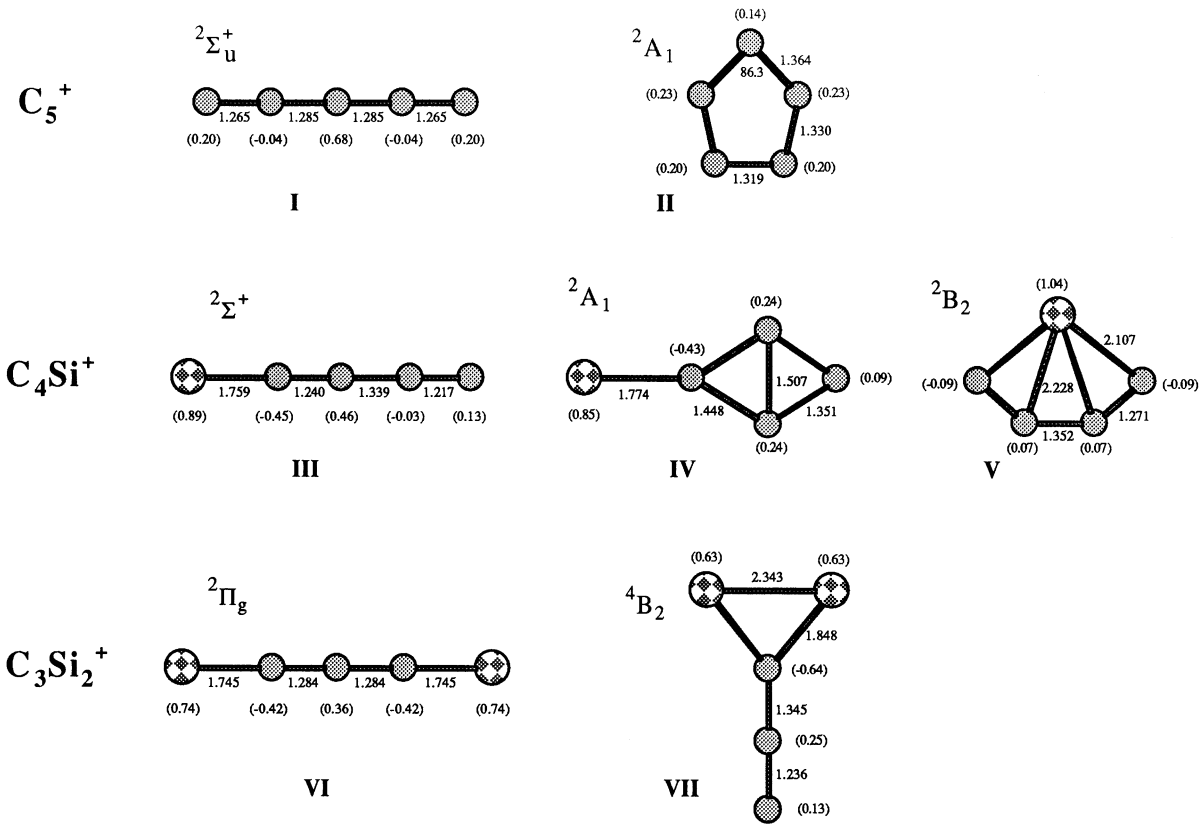

Fig. 1. Equilibrium geometries of energetically low-lying structures of $C_nSi_p^+$ ($n + p = 5$). Distances are in angstroms, angles in degrees, and Mulliken atomic charges (given in parentheses) in electron charge units (e).

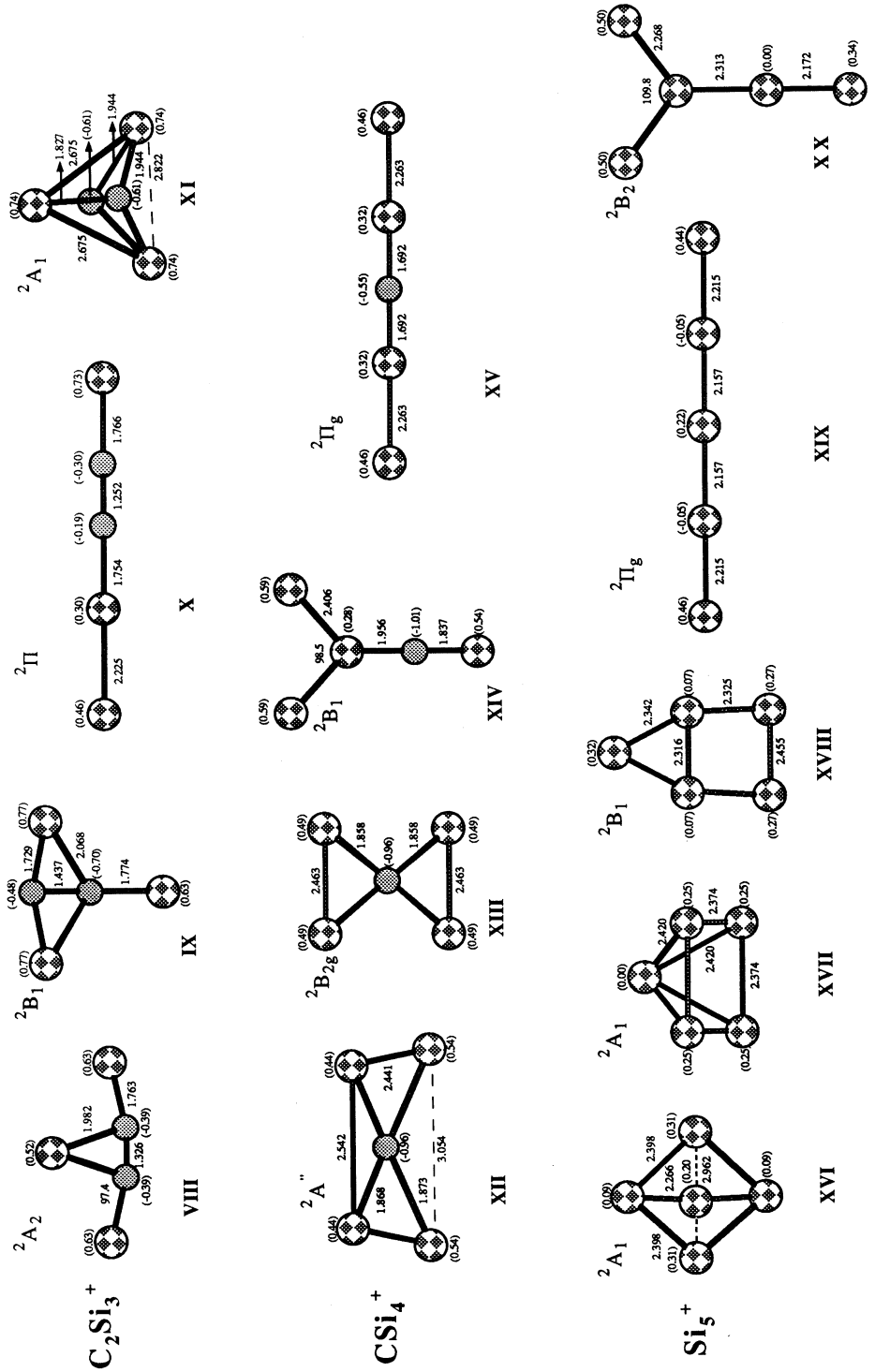

Fig. 1 (*continued*)

Table 1
Valence orbital configurations, total energies (in hartree), relative stabilities ΔE (in kcal · mol^{-1}), and dipole moments (in debye) of the different $C_nSi_p^+$ ($n + p = 5$) structures obtained with the B3LYP/6-311G* method[a]

Isomer	Point group	State	Electronic configuration	ΔE	μ
C_5^+				−189.82715	
I	$D_{\infty h}$	$^2\Sigma_u^+$	core$(\sigma_g)^2(\sigma_u)^2(\sigma_g)^2(\sigma_u)^2(\pi_u)^2(\pi_u)^2(\sigma_g)^2(\sigma_u)^1(\pi_g)^2(\pi_g)^2$	0.0	0.00
II	C_{2v}	$^2A_1$	core$(a_1)^2(a_1)^2(b_2)^2(a_1)^2(b_2)^2(b_1)^2(a_1)^2(a_1)^1(b_1)^2(a_2)^2$	94.5	0.80
C_4Si^+				−441.39836	
III	$C_{\infty v}$	$^2\Sigma^+$	core$(\sigma)^2(\sigma)^2(\sigma)^2(\sigma)^2(\sigma)^2(\pi)^2(\pi)^2(\sigma^1)(\pi)^2(\pi)^2$	0.0	2.15
IV	C_{2v}	$^2A_1$	core$(a_1)^2(a_1)^2(b_2)^2(a_1)^2(b_1)^2(b_2)^2(a_1)^2(a_1)^1(a_1)^1(b_1)^2$	46.2	1.83
V	C_{2v}	$^2B_2$	core$(a_1)^2(b_2)^2(a_1)^2(a_1)^2(b_1)^2(b_2)^2(a_1)^2(b_2)^1(a_1)^2(a_2)^2$	48.0	1.40
$C_3Si_2^+$				−692.91856	
VI	$D_{\infty h}$	$^2\Pi_g$	core$(\sigma_g)^2(\sigma_u)^2(\sigma_g)^2(\sigma_u)^2(\pi_u)^2(\pi_u)^2(\sigma_g)^2(\sigma_u)^2(\pi_g)^2(\pi_g)^1$	0.0	0.00
VII	C_{2v}	$^4B_2$	core$(a_1)^2(a_1)^2(a_1)^2(a_1)^2(b_2)^2(b_1)^2(a_1)^1)(b_2)^2(b_1)^2(b_2)^1(a_1)^1$	80.6	0.67
$C_2Si_3^+$				−944.36548	
VIII	C_{2v}	$^2A_2$	core$(a_1)^2(b_2)^2(a_1)^2(a_1^2(b_1)^2(b_2)^2(a_1)^2(a_1)^2(b_2)^2(a_2)^1$	0.0	0.62
IX	C_{2v}	$^2B_1$	core$(a_1)^2(a_1)^2)(b_2)^2(a_1)^2)b_1)^2(a_1)^2(b_2)^2(a_1)^2(b_2)^2(b_1)^1$	9.9	0.34
X	$C_{\infty v}$	$^2\Pi$	core$(\sigma)^2(\sigma)^2(\sigma)^2(\sigma^2(\pi)^2(\pi)^2\sigma)^2(\sigma)^2(\pi)^2(\pi)^1$	39.7	1.19
XI	C_{2v}	$^2A_1$	core$(a_1)^2(b_1)^2(a_1)^2(b_2)^2(a_1)^2(b_1)^2(a_2)^2(a_1)^2(a_1)^1(b_2)^2$	63.7	1.17
CSi_4^+				−1195.78799	
XII	C_s	$^2A''$	core$(a')^2(a'')^2(a')^2(a')^2(a'')^2(a')^2(a'')^2(a')^2(a')^2(a'')^1$	0.0	0.12
XIII	D_{2h}	$^2B_{2g}$	core$(a_g)^2(b_{1u})^2(b_{2u})^2(a_g)^2(b_{3u})^2(b_{3u})^2(b_{1u})^2(b_{2u})^2(a_g)^2(b_{2g})^1$	0.45	0.00
XIV	C_{2v}	$^2B_1$	core$(a_1)^2(a_1)^2(b_2)^2(a_1)^2(a_1)^2(b_1)^2(b_2)^2(a_1)^2(b_2)^2(b_1)^1$	3.9	0.07
XV	$D_{\infty h}$	$^2\Pi_g$	core$(\sigma_g)^2(\sigma_u)^2(\sigma_g)^2(\sigma_u)^2(\pi_u)^2(\pi_u)^2(\sigma_g)^2(\sigma_u)^2(\pi_g)^2(\pi_g)^1$	78.8	0.60
Si_5^+				−1447.19527	
XVI	C_{2v}	$^2A_1$	core$(a_1)^2(b_1)^2(b_2)^2(a_1)^2(a_1)^2(a_1)^2(b_1)^2(a_2)^2(a_1)^1)(b_2)^2$	0.0	0.31
XVII	C_{4v}	$^2A_1$	core$(a_1)^2(e)^2(e)^2(a_1)^2(b_2)^2(b_1)^2(a_1)^2(e)^2(e)^2(a_1)^1$	12.1	0.46
XVIII	C_{2v}	$^2B_1$	core$(a_1)^2(a_1)^2(b_2)^2(a_1)^2(b_2)^2(a_1)^2(b_1)^2(a_1)^2(b_2)^2(b_1)^1$	19.6	0.06
XIX	$D_{\infty h}$	$^2\Pi_g$	core$(\sigma_g)^2(\sigma_u)^2(\sigma_g)^2(\sigma_u)^2(\sigma_g)^2(\sigma_u)^2(\pi_u)^2(\pi_u)^2(\pi_g)^2(\pi_g)^1$	64.7	0.00
XX	C_{2v}	$^2B_2$	core$(a_1)^2(a_1)^2(b_2)^2(a_1)^2(a_1)^2(b_2)^2(a_1)^2(b_1)^2(b_2)^1(b_1)^2$	67.0	3.36

[a]The symmetry (point group) and the electronic state of the different structures are also given.

quency. The Si–C bond with a length of 1.77 Å is typical of a double Si–C bond and is highly ionic. The C_4 subsystem is similar to the bicyclic structure representing the ground state of the neutral C_4. The Si-capped bent C_4 chain (structure V, C_{2v}) is quasi-energetic with structure IV, the energy difference being only of the order of 2 kcal · mol^{-1}. In structure V, we can notice, however, that the silicon bears the totality of the positive charge (1.04*e*) and the carbon chain is quasineutral (the atomic charge is smaller than 0.1*e* on each carbon). Again, this structure corresponds to a saddle point on the potential energy surface.

3.3. $C_3Si_2^+$

The lowest energy $C_3Si_2^+$ isomer (structure VI, $D_{\infty h}$) is the linear arrangement of nuclei in the $^2\Pi_g$ electronic state. Two double C–C bonds (∼1.28 Å) are formed and the silicon atoms are in the terminal positions. The Si–C bonds (∼1.74 Å), strongly polarized, are also typical of double bonds. The next $C_3Si_2^+$ isomer in the energy ordering, at about 81 kcal · mol^{-1} above the ground state, is found to be a quadruplet $^4B_2$ with a T-shaped geometry (structure VII, C_{2v}). The frequencies are all real for this isomer, which is a local minimum on the potential energy surface. The C–C bonds (1.24 and 1.34 Å) are typical of moderately strong double bonds, and the Si–C bonds (∼1.85 Å) are single bonds. Likewise, the Si–Si bond length of 2.34 Å is indicative of single bonding. The monocyclic C_{2v} isomer (not reported in Table 1) is located higher in energy and rearranges without activation to the linear one.

Table 2
Vibrational frequencies and dipole moments (in debye) of the different $C_nSi_p^+$ ($n + p = 5$) clusters calculated with the B3LYP/6-311G* method[a]

Structure	Vibrational frequencies (cm^{-1})	Zero-point energy (kcal/mol)	Hessian index
C_5^+			
I	156(π_u)^d 267(π_g)^d 626(π_u)^d 804(σ_g) 1586(σ_u) 2092(σ_g) 3010(σ_u)	13.7	0
II	1170i(a2) 717i(b1) 450i(b2) 768(a1) 1150(b2) 1283(a1) 1513(b2) 1515(a1) 1607(a1)	11.2	3
C_4Si^+			
III	91(π)^d 228(π)^d 495(π)^d 544(σ) 1125(σ) 2079(σ) 2221(σ)	10.8	0
IV	408i(b1) 153(b2) 186(b1) 418(b2) 527(a1) 915(b2) 922(a1) 1431(a1) 1637(a1)	8.8	1
V	484i(b1) 209i(b2) 344(a1) 349(b2) 441(a1) 467(a2) 1122(a1) 1683(b2) 1941(a1)	9.1	2
$C_3Si_2^+$			
VI	79(π_u)^d 187(π_g)^d 443(σ_g) 498(π_u)^d 812(σ_u) 1535(σ_g) 1878(σ_u)	8.8	0
VII	142(b2) 225(b1) 307(a1) 439(b2) 546(a1) 685(b2) 1289(a1) 1872(b1) 1995(a1)	10.7	0
VIII	103(a1) 122(b2) 124(b1) 348(a2) 441(a1) 538(b2) 591(a1) 911(b2) 1632(a1)	6.9	0
IX	50(b2) 132(b1) 231(a1) 326(b1) 424(b2) 477(a1) 635(a1) 1046(b2) 1200(a1)	6.5	0
X	67i/41i(π) 99/105(π) 282/319(π) 325(σ) 565(σ) 872(σ) 1959(σ)	6.5	2
XI	250(a1) 295(a2) 296(b2) 325(b2) 405(b1) 414(a1) 647(b1) 696(a1) 818(a1)	5.9	0
CSi_4^+			
XII	81(a″) 81(a′) 150(a′) 218(a″) 308(a″) 317(a′) 463(a′) 787(a″) 837(a′)	4.6	0
XIII	139i(b1) 87i(b2) 99(a2) 200(a1) 280(a1) 316(b2) 461(a1) 810(a1) 873(b2)	4.3	2
XIV	399i(b2) 173i(b1) 162(a1) 190(b2) 208(b1) 334(a1) 462(a1) 732(a1) 829(b2)	4.2	2
XV	66i/43i(π_u) 30i/19(π_g) 128/134(π_u) 282(σ_g) 441(σ_u) 658(σ_g) 1272(σ_u)	4.2	3
Si_5^+			
XVI	132(a1) 186(b2) 219(a1) 240(b2) 279(b1) 285(a2) 384(a1) 433(b1) 474(a1)	3.8	0
XVII	213i(b2) 207(e) 210(b2) 308(a1) 369(b1) 394(e) 458(a1)	3.6	1
XVIII	234i(b2) 35(a2) 38(b1) 217(b2) 291(a1) 339(a1) 406(a1) 418(b2) 485(a1)	3.2	1
XIX	114i/109i(π_u) 64i/48i(π_g) 16/29(π_u) 233(σ_g) 419(σ_u) 573(σ_g) 626(σ_u)	2.7	4
XX	64i(b2) 44i(b1) 14(b2) 56(a1) 168(b1) 253(a1) 453(a1) 487(b2) 527(a1)	2.9	2

[a]Imaginary frequencies indicate a saddle point on the energy surface. The Hessian index and the ZPE are also given.

3.4. $C_2Si_3^+$

Table 1 shows that the $C_2Si_3^+$ cation has an Si-capped symmetrical bent chain in its ground state (structure VIII, C_{2v}). In the SiC_2Si chain, the C–C and Si–C distances (respectively 1.33 Å and 1.76 Å) have typical double bond values and the Si atoms take the terminal positions. The Si–C distances (~1.98 Å) from the capping silicon to the carbons are indicative of weak single bonding. Likewise, the Si–Si distances (~2.82 Å) from this apical silicon to the Si atoms of the chain are typical of very weak single bonds. We can conclude that this isomer can be built from a neutral C_2Si_2 cluster interacting with a silicon in its ionic form. Structure IX located at about 10 kcal · mol^{-1} above the ground state appears as a Si-capped bicyclic ring in the $^2B_1$ state. This isomer has real frequencies and is a local minimum on the potential energy surface. The next structures in the energy ordering are the linear $^2\Pi$ (structure X, $C_{\infty v}$), lying at about 40 kcal · mol^{-1}, and the bipyramid (structure XI, C_{2v}) still much higher in energy, lying at about 64 kcal · mol^{-1} above the ground state. All these structures (VIII, IX, and XI), except X, have real frequencies and are local minima on the potential energy surface.

Table 3
Rotational constants (in GHz) for the most stable $C_nSi_p^+$ isomers ($n + p = 5$)

Structures	A	B	C
I	0.000	2.584	2.584
III	0.000	1.512	1.512
VI	0.000	0.914	0.914
VIII	9.043	1.535	1.312
XII	3.054	2.285	1.309
XVI	2.015	1.933	1.788

3.5. CSi_4^+

As shown in Table 1, two structures are in competition for the ground state: a quasirhombus Si ring capped in its center by a carbon atom (structure XII, C_s) and a very similar, but planar, structure with the carbon atom lying at the center of the Si_4 subsystem (structure XIII, D_{2h}). The nonplanar isomer is favored by an insignificant quantity ~0.4 kcal · mol^{-1}. In these two structures, the Si_4 square bears the positive charge, equally distributed over the four silicon atoms ($0.44e$ to $0.54e$). The carbon atom is quasianionic, bearing a strong negative charge ($-0.96e$), and the Si–C bonds are highly polarized. Differences between these structures essentially reside in the number of Si–Si bonds, two single bonds (2.46 Å) in the planar isomer and three in the nonplanar one (2.44 and 2.54 Å). Structure XIII is not a local minimum and possesses two imaginary frequencies (b1 and b2). The b2 (87i) frequency corresponds to an out-of-plane distortion that ultimately leads to the nonplanar structure XII.

The T-shaped $^2B_1$ isomer (structure XIV, C_{2v}) lies just above the ground state at 4 kcal · mol^{-1}, but this structure with two imaginary frequencies is a saddle point on the energy surface. The linear $^2\Pi_g$ isomer (structure XV, $D_{\infty h}$), with the Si atoms in an outer position, is a high-lying state, located at 79 kcal · mol^{-1} above the global minimum. Again, this structure with three imaginary π frequencies is a saddle point of higher order on the energy surface.

3.6. Si_5^+

Our results give a $^2A_1$ ground state with a distorted trigonal bipyramidal geometry (structure XVI, C_{2v}). Calculations by Raghavachari [31] also suggested a quasisimilar structure for the ground state of the neutral Si_5, but with a D_{3h} symmetry. When ionized, the symmetry of the neutral structure (D_{3h}) is broken into a C_{2v} symmetry. The distances between an Si atom of the base and an apical Si atom is 2.40 Å, typical of a single Si–Si bond. Besides, whereas the distance between two atoms forming the base is very large (2.96 and 3.24 Å), suggesting that these atoms are not bound to each other, the distance between the apical atoms is rather short, ~2.30 Å, typical of a single bond. Hence, structure XVI corresponds to a strongly compressed trigonal bipyramid with a loose interaction between the atoms of the base and a fairly strong interaction between the apical atoms. Given the net charge is essentially distributed—but not equally—over the three Si atoms of the base ($0.31e$ and $0.19e$), with a very weak charge over the apical Si atoms ($0.09e$), this geometry could possibly be linked to the ionic nature of Si_5^+, but the corresponding distances are similar in the neutral [31]. Next in the energy ordering is structure XVII (tetragonal pyramid). This isomer is located at 12 kcal · mol^{-1} above the ground state. The Si–Si bond lengths are all indicative of single bonding (2.37 and 2.40 Å). Vibrational analysis shows that this structure is a saddle point on the energy surface with one imaginary frequency (b2). Other isomers presented in Fig. 1 are the planar edge-capped square (structure XVIII), the linear $^2\Pi_g$ (structure XIX, $D_{\infty h}$) and the T-shaped structure XX. The linear $^2\Pi_g$ state is located higher in energy at about 65 kcal · mol^{-1} above the ground state. This structure possesses four imaginary frequencies, clearly indicating that bending distortions give rise to lower energies.

4. Hexa-atomic silicon-carbon clusters

The equilibrium geometries obtained for the low-energy $C_nSi_p^+$ ($n + p = 6$) isomers are given in Fig. 2; bond lengths, bond angles, and Mulliken atomic charges are also indicated. The electronic states, valence orbital configurations, energies, and dipole moments are listed in Table 4. In Table 5, the vibrational frequencies and zero-point corrections for these compounds are listed. In Table 6, the rotational constants of the ground state isomers are given.

4.1. C_6^+

From Fig. 2, we find the linear $^2\Pi_u$ as the ground state of C_6^+ (structure I, $D_{\infty}h$). The C–C bond lengths (1.34, 1.26, and 1.31 Å) are indicative of cumulenic bonding. The two median carbons bear the positive

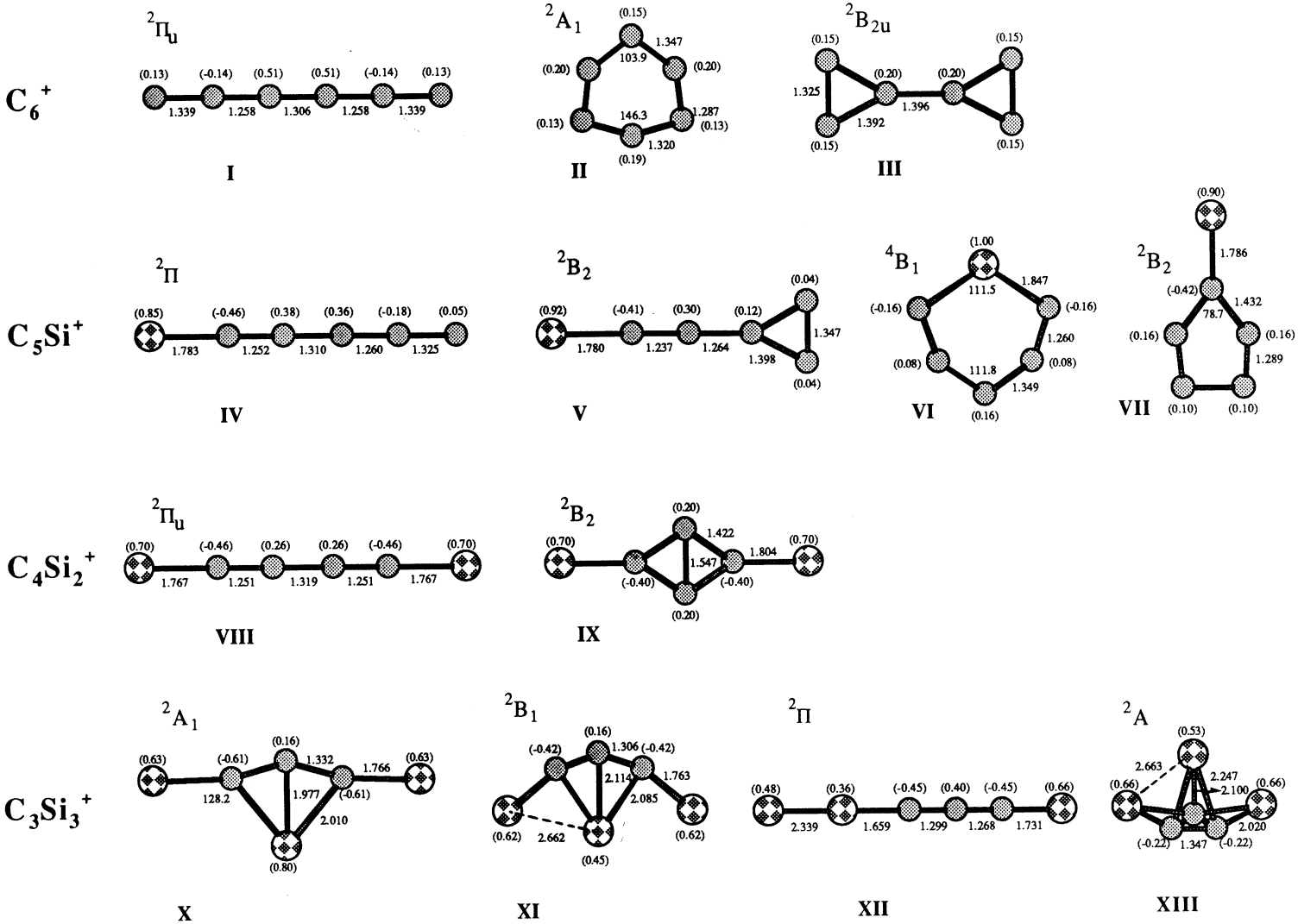

Fig. 2. Equilibrium geometries of energetically low-lying structures of $C_nSi_p^+$ ($n + p = 6$). Distances are in angstroms, angles in degrees, and Mulliken atomic charges (given in parentheses) in electron charge units (e).

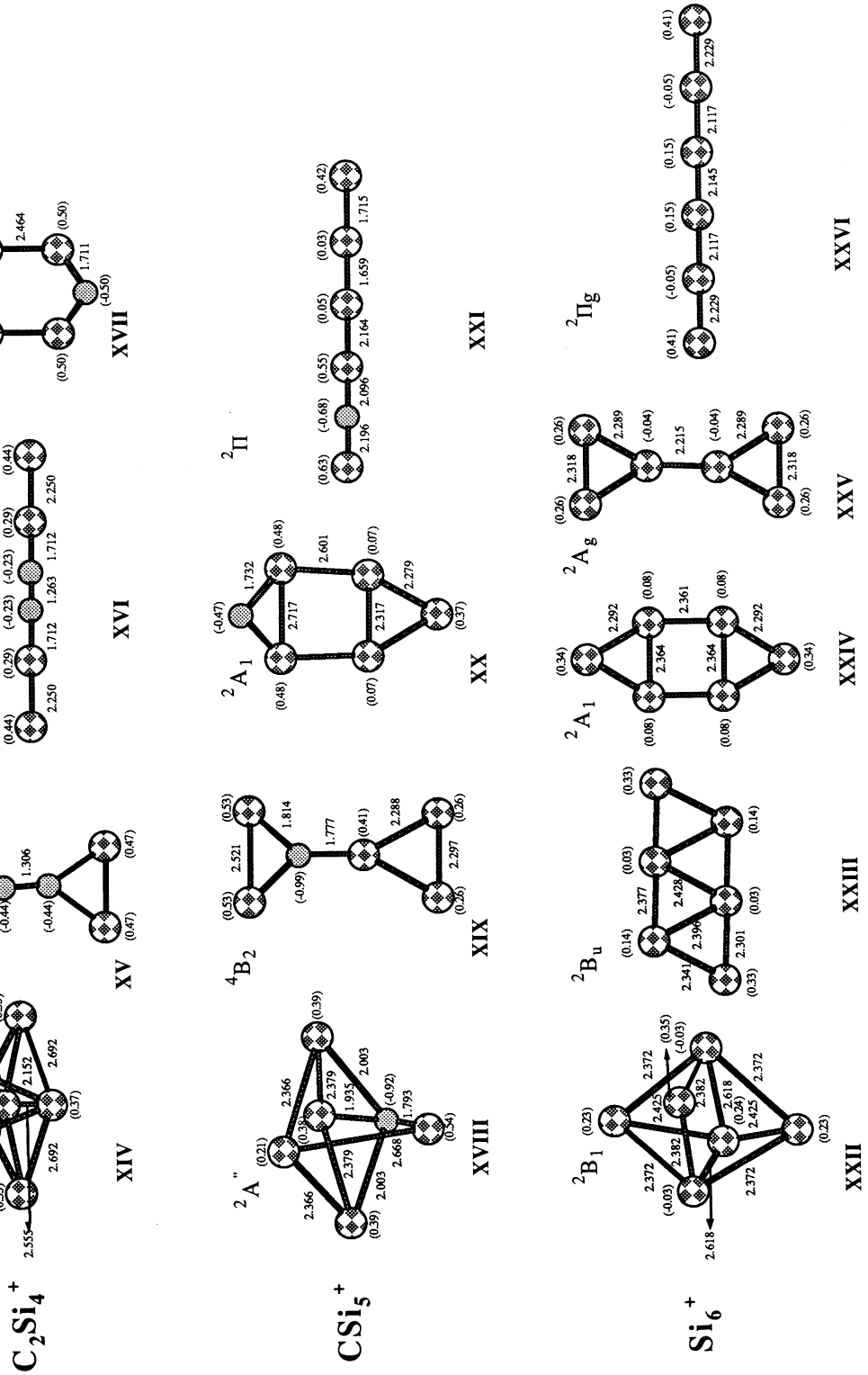

Fig. 2 (*continued*)

Table 4
Valence orbital configurations, total energies (in hartree), relative stabilities ΔE (in kcal · mol^{-1}), and dipole moments (in debye) of the different $C_nSi_p^+$ ($n + p = 6$) structures obtained with the B3LYP/6-311G* method[a]

Isomer	Point group	State	Electronic configuration	ΔE	μ
C_6^+				−227.94142	
I	$D_{\infty h}$	$^2\Pi_u$	core$(\sigma_g)^2(\sigma_u)^2(\sigma_g)^2(\sigma_u)^2(\sigma_g)^2(\pi_u)^2(\pi_u)^2(\pi_g)^2(\pi_g)^2(\sigma_u)^2(\sigma_g{}^2)(\pi_u)^1$	0.0	0.00
II	C_{2v}	$^2A_1$	core$(a_1)^2(b_2)^2(a_1)^2(b_2)^2(a_1)^2(b_2)^2(a_1)^2(b_1)^2(a_1)^1(a_2)^2(b_2)^2(b_1)^2$	10.5	0.82
III	D_{2h}	$^2B_{2u}$	core$(a_g)^2(b_{1u})^2(a_g)^2(b_{2u})^2(b_{1u})^2(b_{3g})^2(a_g)^2(b_{3u})^2(b_{2g})^2(b_{1u})^2(a_g)^2(b_{2u})^1$	49.8	0.00
C_5Si^+				−479.49144	
IV	$D_{\infty h}$	$^2\Pi$	core$(\sigma)^2(\sigma)^2(\sigma)^2(\sigma)^2(\sigma)^2(\pi)^2(\pi)^2(\sigma)^2(\pi)^2(\pi^2(\sigma)^2(\pi)^1$	0.0	5.74
V	C_{2v}	$^2B_2$	core$(a_1)^2(a_1)^2(a_1)^2(a_1)^2(b_2)^2(a_1)^2(b_1)^2(b_2)^2(a_1)^2(b_1)^2(a_1)^2(b_2)^1$	20.8	6.45
VI	C_{2v}	$^4B_1$	core$(a_1)^2(b_2)^2(a_1)^2(b_2)^2(a_1)^2(b_2)^2(a_1)^2(b_1)^2(a_2)^2(b_2)^2(a_1)^1(a_1)^1(b_1)^1$	51.0	1.50
VII	C_{2v}	$^2B_2$	core$(a_1)^2(a_1)^2(b_2)^2(a_1)^2(b_2)^2(a_1)^2(b_1)^2(a_1)^2(a_1)^2(b_2)^1(b_1)^2(a_2)^2$	85.4	4.10
$C_4Si_2^+$				−731.02022	
VIII	$D_{\infty h}$	$^2\Pi_u$	core$(\sigma_g)^2(\sigma_u)^2(\sigma_g)^2(\sigma_u)^2(\sigma_g)^2(\pi_u)^2(\pi_u)^2(\sigma_u)^2(\sigma_g)^2(\pi_g)^2(\pi_g)^2(\pi_u)^1$	0.0	0.00
IX	C_{2v}	$^2B_2$	core$(a_1)^2(a_1)^2(a_1)^2(b_2)^2(a_1)^2(b_1)^2(b_2)^2(a_1)^2(a_1)^2(a_1)^2(b_1)^2(b_2)^1$	71.9	0.00
$C_3Si_3^+$				−982.43065	
X	C_{2v}	$^2A_1$	core$(a_1)^2(b_2)^2(a_1)^2(b_2)^2(a_1)^2(b_1)^2(b_2)^2(a_1)^2(a_1)^2(b_2)^2(a_2)^2(a_1)^1$	0.0	1.27
XI	C_{2v}	$^2B_1$	core$(a_1)^2(b_2)^2(a_1)^2(b_2)^2(a_1)^2(b_1)^2(a_1)^2(b_2)^2(b_2)^2(a_1)^2(a_2)^2(b_1)^1$	7.5	1.05
XII	$C_{\infty v}$	$^2\Pi$	core$(\sigma)^2(\sigma)^2(\sigma)^2(\sigma)^2(\sigma)^2(\pi)^2(\pi)^2(\sigma)^2(\sigma)^2(\sigma)^2(\pi)^2(\pi)^1$	15.1	1.90
XIII	C_s	$^2A'$	core$(a')^2(a'')^2(a')^2(a')^2(a')^2(a')^2(a'')^2(a')^2(a''^2)(a')^2(a'')^2(a')^1$	22.6	1.12
$C_2Si_4^+$				−1233.87753	
XIV	C_{2v}	$^2A_1$	core$(a_1)^2(b_2)^2(a_1)^2(b_1)^2(a_1)^2(a_1)^2(b_2)^2(b_1)^2(a_1)^2(a_2)^2(b_2)^2(a_1)^1$	0.0	0.68
XV	D_{2h}	$^2B_{1u}$	core$(a_g)^2(b_{1u})^2(a_g)^2(b_{2u})^2(b_{3g})^2(b_{1u})^2(b_{3u})^2(a_g)^2(b_{2u})^2(b_{2g})^2(a_g)^2(b_{1u})^1$	36.2	0.00
XVI	$D_{\infty h}$	$^2\Pi_u$	core$(\sigma_g)^2(\sigma_u)^2(\sigma_g)^2(\sigma_u)^2(\sigma_g)^2(\pi_u)^2(\pi_u)^2(\sigma_u)^2(\sigma_g)^2(\pi_g)^2(\pi_g)^2(\pi_u)^1$	72.0	0.00
XVII	D_{2h}	$^2B_{1u}$	core$(a_g)^2(b_{1u})^2(b_{2u})^2(b_{3g})^2(a_g)^2(b_{2u})^2(a_g)^2(b_{1u})^2(b_{3u})^2(b_{2g})^2(b_{1u})^1(b_{3u})^2$	90.1	0.00
CSi_5^+				−1485.31438	
XVIII	C_s	$^2A''$	core$(a')^2(a')^2(a'')^2(a')^2(a')^2(a')^2(a'')^2(a')^2(a'')^2(a')^2(a'')^1$	0.0	0.18
XIX	C_{2v}	$^4B_2$	core$(a_1)^2(a_1)^2(a_1)^2(b_2)^2(b_2)^2(a_1)^2(a_1)^2(b_1)^2(b_2)^2(a_1)^1(b_1)^2(b_2)^1(a_1)^1$	39.2	0.95
XX	C_{2v}	$^2A_1$	core$(a_1)^2(a_1)^2(b_2)^2(a_1)^2(b_2)^2(a_1)^2(b_2)^2(a_1)^2(b_1)^2(b_1)^2(a_1)^2(a_1)^1$	71.1	1.90
XXI	$C_{\infty v}$	$^2\Pi$	core$(\sigma)^2(\sigma^2(\sigma)^2(\sigma)^2(\sigma)^2(\sigma)^2(\pi)^2(\pi)^2(\pi)^2(\pi)^2(\pi)^1$	93.3	1.32
Si_6^+				−1736.74506	
XXII	C_{2v}	$^2B_1$	core$(a_1)^2(a_1)^2(b_1)^2(b_2)^2(a_1)^2(a_1)^2(b_1)^2(b_2)^2(a_2)^2(a_1)^2(a_1)^2(b_1)^1$	0.0	0.19
XXIII	C_{2h}	^2B_u	core$(a_g)^2(b_u)^2(b_u)^2(a_g)^2(a_g)^2(b_u)^2(a_g)^2(a_u)^2(b_u)^2(a_g)^2(b_g)^2(b_u)^1$	21.3	0.00
XXIV	C_{2v}	$^2A_1$	core$(a_1)^2(a_1)^2(b_2)^2(a_1)^2(b_2)^2(a_1)^2(a_1)^2(b_1)^2(b_2)^2(a_1)^2(b_1)^2(a_1)^1$	32.2	0.00
XXV		^2A_g	core$(a_g)^2(b_{1u})^2(a_g)^2(b_{2u})^2(b_{3g})^2(b_{1u})^2(a_g)^2(b_{3u})^2(b_{2g})^2(b_{1u})^2(a_g)^1(b_{2u})^2$	64.4	0.00
XXVI	$D_{\infty h}$	$^2\Pi_g$	core$(\sigma_g)^2(\sigma_u)^2(\sigma_g)^2(\sigma_u)^2(\sigma_g)^2(\sigma_u)^2(\sigma_g)^2(\pi_u)^2(\pi_u)^2(\pi_g)^2(\pi_g)^2(\pi_u)^1$	112.2	0.00

[a]The symmetry (point group) and the electronic state of the different structures are also given.

charge ($0.51e$). The monocyclic ring (structure II, C_{2v}) lies 10 kcal · mol^{-1} above the ground state. The charge is equally distributed along the ring. These two isomers represent local minima on the potential energy surface. However, the energy ordering is different for the neutral C_6, where the cyclic ring is predicted to be more stable than the linear by about 10 kcal · mol^{-1}. (see Weltner and Van Zee [32] for a detailed discussion on the neutral C_n). Moreover, the neutral monocyclic ring is found to be of D_{3h} symmetry. Again, we assist a symmetry breaking ($D_{3h} \rightarrow C_{2v}$) when the ring is ionized. Possibly the energy ordering inversion between the linear and the monocyclic ring, as well as the symmetry breaking, are both linked to an electrostatic charge effect. A strained formlike structure III with two opposite triangles also represents a local minimum on the energy surface, even though this isomer is relatively high in energy (at ~50 kcal · mol^{-1} above the ground state).

4.2. C_5Si^+

In terms of energetic behaviour, the most favorable isomer C_5Si^+ is the linear $^2\Pi$ (structure IV, $C_{\infty v}$). The

Table 5
Vibrational frequencies (in cm^{-1}) and dipole moments (in debye) of the different $C_nSi_p^+$ ($n + p = 5$) clusters calculated with the B3LYP/6-311G* method[a]

Structure	Vibrational frequencies	Zero-point energy (kcal/mol)	Hessian index
C_6^+			
I	83/93(π_g) 153/163(π_u) 303/332(π_g) 360/610(π_u) 659(σ_g) 1164(σ_u) 1576(σ_g) 2062(σ_u) 2193(σ_g)	13.9	0
II	396(b1) 479(a2) 492(b1) 557(a1) 670(a1) 709(b2) 1193(a1) 1238(a1) 1309(b2) 1541(b2) 1768(a1) 2226(b2)	18.0	0
III	131(a_u) 146(b2u) 210(b3u) 462(b3g) 569(b2g) 620(ag) 893(b3g) 1211(b2u) 1219(b1u) 1508(ag) 1597(b1u) 1750(ag)	14.7	0
C_5Si^+			
IV	72/79(π) 157/181(π) 317/343(π) 428/655(π) 471(σ) 908(σ) 1476(σ) 2021(σ) 2137(σ)	13.2	0
V	446i(b2) 86(b1) 91(b2) 254(b1) 257(b2) 466(a1) 538(b2) 549(b1) 928(a1) 1270(a1) 1645(a1) 2111(a1)	11.7	1
VI	139($b2$) 310($a1$) 323($b1$) 363($a2$) 481($b1$) 583($a1$) 706($b2$) 711($a1$) 1092($a1$) 1289($b2$) 1704($b2$) 1832($a1$)	13.6	0
VII	340i(a2) 302i(b2) 122(b1) 148(b2) 386(b1) 479(a1) 786(a1) 818(b2) 1045(a1) 1338(a1) 1604(b2) 1729(a1)	12.1	2
$C_4Si_2^+$			
VIII	61/67(π_g) 142/167(π_u) 318/349(π_g) 396(σ_g) 505/662(π_u) 667(σ_u) 1204(σ_g) 1969(σ_u) 2103(σ_g)	12.3	0
IX	75(b1) 122(b2) 227(b1) 257(b2) 386(a1) 548(b1) 566(a1) 575(b2) 613(b2) 950(a1) 1404(a1) 1415(a1)	10.2	0
$C_3Si_3^+$			
X	58(b1) 104(a1) 115(b2) 221(a2) 279(b2) 380(a1) 488(a1) 499(b1) 699(a1) 700(b2) 1388(a1) 1596(b2)	9.3	0
XI	6(b1) 109(a1) 180(b2) 217(a2) 288(a1) 357(b2) 372(b1) 566(a1) 683(a1) 754(b2) 1493(a1) 1695(b2)	9.8	0
XII	92i/11(π) 74/79(π) 190/214(π) 272(σ) 485(σ) 524/590(π) 904(σ) 1546(σ) 2007(σ)	8.8	1
XIII	135(a') 172(a'') 192(a') 300(a') 331(a'') 348(a'') 448(a') 520(a') 596(a'') 784(a'') 795(a') 1522(a')	8.6	0
$C_2Si_4^+$			
XIV	123(a1) 126(b1) 151(a2) 231(b2) 238(a1) 332(b1) 380(a1) 421(a2) 528(b2) 581(a1) 881(b2) 1589(a1)	8.0	0
XV	167i(b2u) 80(au) 135(b3u) 236(b3g) 265(ag) 325 (b2u) 413(b1u) 444(b2g) 491(ag) 881(b1u) 1048(b3g) 1617(ag)	8.5	1
XVI	54i/43i(π_u) 37i(π_g)[d] 107/110(π_g) 265(σ_g) 331/397(π_u) 400(σ_u) 618(σ_g) 997(σ_g) 1874(σ_g)	7.3	4
XVII	399i($b2g$) 324i($b1u$) 157i(au) 129i($b3g$) 118($b3u$) 193(ag) 256($b2u$) 345(ag) 769($b1u$) 810(ag) 1084($b3g$) 1127($b2u$)	6.7	4
CSi_5^+			
XVIII	116(a') 134(a') 187(a') 220(a') 280(a') 357(a'') 359(a'') 368(a') 432(a') 537(a') 545(a'') 906(a')	6.3	0
XIX	16i(a2) 64(b2) 84(b1) 192(b2) 199(a1) 277(b1) 308(a1) 404(b2) 422(a1) 594(a1) 679(b2) 1063(a1)	6.1	1
XX	113i(b2) 70i(a2) 68i(b2) 71(b1) 167(a1) 206(b1) 255(a1) 314(a1) 368(b2) 492(a1) 793(a1) 972(b2)	5.2	3
XXI	235i/134i(π) 14/18(π) 46/57(π) 123(π)[d] 230(σ) 403(σ) 590(σ) 682(σ) 1383(σ)	5.2	2
Si_6^+			
XXII	73(b1) 83(b2) 153(a1) 301(a1) 305(b2) 308(b1) 334(a1) 352(b2) 370(a2) 405(a1) 411(b1) 441(a1)	5.1	0
XXIII	57(au) 83(au) 148(bu) 151(bg) 218(ag) 281(ag) 318(bu) 332(ag) 379(bu) 406(ag) 490(bu) 503(ag)	4.8	0
XXIV	162i(b2) 133i(a2) 66(b1) 135(b2) 146(b1) 274(a1) 288(a1) 312(b2) 397(a1) 482(b2) 553(a1)	4.5	2
XXV	15i($b3g$) 22($b2u$) 43($b3u$) 64(au) 111($b2g$) 201(ag) 297($b3g$) 329($b1u$) 408(ag) 465($b2u$) 494($b1u$) 591(ag)	4.3	2
XXVI	202i/139i(π_u) 89i(π_g) 21i/27(π_u) 20(π)[d] 205(σ_g) 365(σ_u) 492(σ_g) 621(σ_u) 700(σ_g)	3.5	5

[a]Imaginary frequencies indicate a saddle point on the energy surface. The Hessian index and the ZPE are also given.

Table 6
Rotational constants (in GHz) for the most stable $C_nSi_p^+$ isomers ($n + p = 6$)

Structures	A	B	C
I	0.000	1.438	1.438
IV	0.000	0.911	0.911
VIII	0.000	0.591	0.591
X	8.853	0.914	0.828
XIV	3.686	1.497	1.319
XVIII	1.919	1.730	1.361
XXII	1.706	1.406	1.179

C–C bond lengths alternate between normal double bonds (1.31 and 1.32 Å) and strong double bonds (1.25 and 1.26 Å). The Si–C bond is typical of a double bond (1.78 Å), giving the molecule a cumulenelike structure. The silicon atom occupies the terminal position and bears the positive charge ($0.85e$).

The T-shaped geometry (structure V, C_{2v}) possesses a triangular C_3, in which the carbons are bound to each other by C–C double bonds, increasing the number of these bonds with respect to the linear species. But this strongly strained form lies at 21 kcal · mol^{-1} above the linear and possesses one imaginary frequency (b_2). The monocyclic isomer (structure VI, C_{2v}) is a local minimum on the energy surface but is located higher in energy, at 51 kcal · mol^{-1} above the ground state. Other geometries like the Si-capped pentagon are located much higher in energy.

4.3. $C_4Si_2^+$

Table 4 indicates that the lowest energy isomer of $C_4Si_2^+$ has a linear SiC_4Si geometry in the $^2\Pi_u$ ground state. This structure was however foreseeable, given that a linear arrangement of nuclei is already predicted for the neutral C_4Si_2 [33,34]. This structure is quite similar to the linear C_6^+ ($^2\Pi_u$), excepting the atomic charge distribution. In C_6^+, the positive charge is located on the two median carbons ($0.51e$), whereas in $C_4Si_2^+$, the terminal silicons bear the positive charge ($0.70e$). The next low-lying structure is predicted to be a Si-bicapped bicyclic C_4 structure located at 72 kcal · mol^{-1} above the linear ground state. The monocyclic ring was also considered but this one gives rise to a linear configuration by rearrangement.

4.4. $C_3Si_3^+$

Clearly contrasting with the preceding clusters ($C_nSi_p^+$ with $n > p$), in the case of $C_3Si_3^+$, the linear isomer (structure XII, $D_{\infty h}$) is found to be less stable than the planar structure X by 15 kcal · mol^{-1}. Moreover, vibrational analysis shows that the linear has one imaginary π frequency, indicating that this state is not a local minimum.

The global minimum energy isomer (structure X, C_{2v}) is composed of a distorted SiC_3Si chain capped by an Si atom. The C–C and Si–C bonds in the basal five-membered SiC_3Si chain, with respective lengths of 1.33 and 1.77 Å, are typical of double bonds. The bonds between the capping silicon and the carbons of the chain appear as weak single bonds (2.01 and 1.98 Å). There exists another very similar structure (XI, C_{2v}) located just above structure X in energy, at about 7.5 kcal · mol^{-1}. Structure XI is also a local minimum. The energy difference appearing between these two isomers, however, is most likely linked to the atomic charge distribution. For structure X, two of the three bonds between the capping silicon and the carbons are strongly polarized (Fig. 2), the capping silicon having a strong positive charge ($0.80e$). These bonds are less polarized in structure XI, the charge on the silicon being of the order of $0.45e$.

The three-dimensional structure XIII is located much higher in energy, at 23 kcal · mol^{-1} above the ground state, even though it is a local minimum on the energy surface. At this point, it is interesting to compare it with the neutral C_3Si_3. The ground state of the neutral C_3Si_3 is predicted to be a bipyramidal form analogous to structure XIII [35]. Once again, as for C_6^+, we see that a net positive charge has a destabilizing effect on a multidimensional arrangement such as structure XIII. The global result is a lowering of the dimensionality (3D → 2D).

4.5. $C_2Si_4^+$

The ground state of $C_2Si_4^+$ is found to be the face-capped trigonal bipyramid (structure XIV, C_{2v}). This is similar to the geometry derived for the corresponding neutral species [33]. The four Si atoms are all positively charged ($0.55e$ and $0.37e$), and the two carbons are negatively charged ($-0.42e$). From a simple analysis of the bond distances, we can very roughly decompose this structure into two interacting entities: a weakly charged SiC_2Si bent chain with the Si atoms in the terminal positions and an Si_2 quasi-ionic molecule set perpendicularly to the chain. In the SiC_2Si bent chain, the C–C bond length of 1.32 Å is very close to a double bond. The Si–C bond is highly polarized ($0.55e$ and $-0.42e$), and its length (1.79 Å) is close to a single bond value. Very similar distances were found for the linear $^2\Pi_g$, representing the ground state of $C_2Si_2^+$ [16]. The other subsystem is a positively charged Si_2 structure with a bond length of 2.55 Å. This value is larger than a typical single bond [the bond length in the Si_2^+ ($^4\Sigma_g$) ion is 2.30 Å]. Structure XIV could also be seen as a dicationic Si_4 rhombus (total charge $+1.84e$) interacting with an anionic C_2 entity (total charge $-0.84e$). But in this case, the Si–Si bond length (2.69 Å) in the Si_4 rhombus is considerably larger than a typical single bond.

There exists a strong analogy between the ground state of $C_2Si_3^+$ (structure VIII) and the ground state of $C_2Si_4^+$ (structure XIV). These structures are both built from the same basal arrangement of nuclei (an SiC_2Si chain) capped by one ($C_2Si_3^+$) or two silicon atoms ($C_2Si_4^+$).

The other low-lying isomers of $C_2Si_4^+$ are all located higher in energy, especially the linear chain (XVI, $D_{\infty h}$) located at 72 kcal · mol^{-1} above the ground state. This linear form possesses four imaginary π frequencies, indicating that bonding distortions give rise to lower energies. In the same way, the monocyclic isomer (XVII, D_{2h}), located at 90 kcal · mol^{-1} above the ground state, has four imaginary frequencies (b_{2g}, b_{1u}, a_u, and b_{3g}) showing again the tendency to drive lower-energy structures. A noticeable point of this very symmetrical molecule is that the charge is equally distributed along the ring ($0.50e$ on silicons and $-0.50e$ on carbons).

4.6. CSi_5^+

The lowest-energy CSi_5^+ isomer (structure XVIII) is a three-dimensional arrangement in the $^2A''$ (C_s) electronic state. This structure can be built up from a CSi_4 cationic entity (total charge $0.79e$), similar to a distorted CSi_4^+ cluster in its ground state (structure XII of Fig. 1). The weakly capping silicon (charge $0.21e$) is linked to the basal CSi_4 substructure by three single Si–Si bonds (2.37 Å).

The monocyclic isomer does not properly exist, given that two transannular Si–Si bonds (2.72 and 2.32 Å) now appear in the structure (structure XX, C_{2v}). In any case, this form is located higher in energy, at 71 kcal · mol^{-1} above the ground state and the presence of three imaginary frequencies is indicative of a saddle point of higher order on the energy surface. The linear $^2\Pi$ (structure XXI, $C_{\infty v}$) is found still much higher in energy, at 93 kcal · mol^{-1} above the ground state. The latter isomer possesses two imaginary frequencies, indicating that lower symmetry structures can cause stabilization.

4.7. Si_6^+

The edge-capped trigonal bipyramid (structure XXII, C_{2v}) is found as the ground state of Si_6^+. The corresponding Si–Si bond lengths from one apical Si atom to a basal plane Si atom are very similar whether the cluster is ionized or not, but the Si–Si distances in the basal plane appear a bit larger in the cation (2.38 and 2.62 Å) than in the neutral (2.32 and 2.43 Å in reference [31]). Structure XXII can be built up from a Si_5^+ cluster in its ground state (trigonal bipyramid) by adding a silicon atom in the basal plane. The same structure has been found for the neutral species [28]. Next in the energy ordering is a planar structure (XXIII, C_{2h}) lying at about 21 kcal · mol^{-1} above the ground state. Evaluation of the vibrational frequencies indicates that structure XXIII is also a local minimum on the energy surface. The neutral species corresponding to this structure has a low-lying D_{3d} sym-

Table 7
Build-up principle of the $C_nSi_p^+$ ($n + p = 5,6$) clusters in their ground state[a]

	ΔEb (eV)
$C_2Si_2^+$(linear, $^2\Pi_g$) + Si($^3P_0$) → $C_2Si_3^+$ (VIII, $^2A_2$)	3.94
$C_2Si_3^+$(VIII, $^2A_2$) + Si($^3P_0$) → $C_2Si_4^+$ (XIV, $^2A_1$)	3.21
$C_3Si_2^+$(VI, $^2\Pi_g$) + Si($^3P_0$) → $C_3Si_3^+$ (X, $^2A_1$)	3.22
CSi_3^+(T geometry, $^2B_2$) + Si($^3P_0$) → CSi_4^+(XII, $^2A''$)	3.31
CSi_4^+(XII, $^2A''$) + Si($^3P_0$) → CSi_5^+ (XVIII, $^2A''$)	3.60
Si_4^+(monocyclic ring, $^2B_2$) + Si($^3P_0$) → Si_5^+ (XVI, $^2A_1$)	3.17
Si_5^+(XVI, $^2A_1$) + Si($^3P_0$) → Si_6^+ (XXII, $^2B_1$)	4.24

[a]The various structures are reproduced in Fig. 1 and Fig. 2.[b] ΔE_b denotes the binding energy of added silicon.

[b]The geometries of the $C_2Si_2^+$, CSi_3^+, and Si_4^+ cations are given in reference [19].

metry derived from a crystal fragment [31]. Thus, the ionization induces a symmetry breaking ($D_{3d} \rightarrow C_{2h}$) for this isomer. Starting from a D_{3d} geometry, the monopositive ion rearranges toward a C_{2h} geometry without activation. Other geometries displayed in Fig. 2 are the bicapped square (XXIV, D_{2h}), the double-T-shaped XXV, and the linear (XXVI, $D_{\infty h}$). These structures are respectively located at 32, 64, and 112 kcal · mol^{-1} above the ground state and represent saddle points on the potential energy surface.

5. General discussion

It is of interest to make a comparative study of the two series of $C_nSi_p^+$ ($n + p = 5, 6$) clusters. From Figs. 1 and 2, it can be immediately envisioned that each $C_nSi_p^+$ ($n + p = 6$) cluster can be built up from a $C_nSi_p^+$ ($n + p = 5$) cluster by attaching a Si atom at an appropriate site. For instance, $C_3Si_3^+$ in its ground state can be made from the linear $C_3Si_2^+$ by adding an Si atom perpendicularly to the SiC_3Si chain. Three Si–C bonds are then formed in a process in which the basal linear structure is distorted to make these Si–C bonds equivalent. The same considerations can easily be made for the other ($n + p = 6$) structures in their ground state. We present in Table 7 a series of some possibilities for bridging a $C_nSi_p^+$ cluster with a silicon atom to obtain a $C_nSi_{p+1}^+$ cluster. All the clusters of this list are considered in their ground state. The binding energies of the added silicon ΔE_b are also given. This energy is high for Si_6^+, indicating that this cluster is particularly stable compared with the adjacent Si_5^+ cluster, as suggested from an earlier calculation [31]. From the present study, we can also derive general bonding considerations concerning the stability of the $C_nSi_p^+$ clusters. As is well known, a basic rule for the neutral species is that carbon partakes in multiple bonding, whereas silicon prefers single bonding in higher coordination numbers [33]. Following this important rule, carbon-rich aggregates ($p < n$) adopt linear or planar arrangements and silicon-rich aggregates ($p \geq n$, $p > 3$) adopt three-dimensional structures. Strong C–C bonds are favored over C–Si bonds, whereas Si–Si bonds are less important. This rule also pertains to the ionized clusters, but with a few alterations. The ground state of the neutral C_6 is found to be the monocyclic ring with six C–C bonds [32]. In the ionized form, the ground state is linear, even though this one has only five C–C bonds and possesses terminal dangling bonds as a destabilizing factor. Despite this, the net positive charge causes the monocyclic ring, with all its carbons positively charged, to become less stable than the linear, for which the charge is strongly oscillating along the chain. In the carbon-rich cluster cations ($n > p$, $n + p = 5,6$), the linear isomers are thus always favored over the monocyclic structures (e.g., C_5^+, C_6^+ are linear). This is different in the neutral species, where an even-odd parity effect in the number of atoms can play a determining role in the stability (C_5 is linear, C_6 is cyclic). Another interesting case is C_3Si_3. Three-dimensional structure XIII possesses three C–C bonds and seven Si–C bonds, whereas planar structure X has only two C–C bonds and five C–Si bonds. Following formal considerations relative to the number of C–C and Si–C bonds, three-dimensional structure XIII should be more stable than two-dimensional structure X, as is effectively the case for the corresponding neutral species. In the cation, however, the relative stability is inverted and planar structure X is favored over three-dimensional structure XIII. Thus, a net positive charge can, in a number of situations, reduce the dimensionality of a C_nSi_p ($n + p = 6$) cluster

following the pathway: planar to linear for C_6 and three- to two-dimensional for C_3Si_3. In other words, as soon as it is ionized, the cluster undergoes rearrangement to minimize its electrostatic energy, a process that eventually favors less compact or low-dimensionality structures.

6. Conclusions

The geometries and energies of small penta- and hexa-atomic clusters $C_nSi_p^+$ ($n + p = 5,6$) have been analyzed by a DFT method. Several geometric structures have been investigated for each cluster. The ground state geometries are linear for C_5^+ ($^2\Sigma_u^+$), C_4Si^+ ($^2\Sigma^+$), and $C_3Si_2^+$ ($^2\Pi_g$), a Si-capped SiC_3Si bent chain for $C_2Si_3^+$ ($^2A_2$), a nonplanar C-capped Si square for CSi_4^+ ($^2A''$), and the trigonal bipyramid for Si_5^+ ($^2A_1$). Among the hexa-atomic clusters, the ground state geometries are linear for C_6^+ ($^2\Pi_u$), C_5Si^+ ($^2\Pi$), and $C_4Si_2^+$ ($^2\Pi_u$), the Si-capped SiC_3Si bent chain for $C_3Si_3^+$ ($^2A_1$), and various three-dimensional structures for $C_2Si_4^+$ (face-capped trigonal bipyramid, $^2A_1$), CSi_5^+ ($^2A''$), and Si_6^+ (edge-capped trigonal bipyramid, $^2B_1$). In these mixed silicon-carbon clusters, carbon and silicon atoms have different electronegativities; the structural modifications ongoing from the neutrals to the corresponding cations can be sufficiently important for some clusters to invert the energy ordering in the low-lying isomers. Such inversions generally appear associated with a dimensionality lowering for the monopositive C_nSi_p clusters with respect to the corresponding neutrals, an effect that can ultimately be rationalized in terms of electrostatic energy minimization.

References

[1] J. Cernicharo, C. A. Gottlieb, M. Guelin, P. Thaddeus, J. M. Vrtilek, Astrophys. J. 341 (1989) L25.
[2] D. Williams, in I. Nenner (Ed.), Molecules and Grains in Space, IAP Conference Proceedings 312, 1993, pp. 3–23.
[3] C. T. Pillinger, S. S. Russel, J. Chem. Soc. Faraday Trans. 89 (1993) 2297.
[4] R. S. Grev, H. F. Schaeffer III, J. Chem. Phys. 82 (1985) 4126.
[5] R. S. Grev, H. F. Schaeffer III, J. Chem. Phys. 80 (1984) 3352.
[6] G. W. Trucks, R. J. Bartlet, J. Mol. Struct. (Theochem.) 135 (1986) 423.
[7] V. Sudhakar, O. F. Günner, K. Lammerstma, J. Phys. Chem. 93 (1989) 7289.
[8] K. Lammerstma, O. F. Günner, J. Am. Chem. Soc. 110 (1988) 5239.
[9] C. M. Rittby, J. Chem. Phys. 96 (1992) 6768.
[10] J. D. Presilla-Márquez, W. R. M. Graham, J. Chem. Phys. 96 (1992) 6509.
[11] G. Froudakis, A. D. Zdetsis, J. Chem. Phys. 101 (1994) 6590.
[12] G. Froudakis, M. Mülhaüser, A. D. Zdetsis, Chem. Phys. Lett. 233 (1995) 619.
[13] A. D. Zdetsis, G. Froudakis, M. Mülhaüser, H. Trümmel, J. Chem. Phys. 104 (1996) 2566.
[14] C. E. Richter, M. Trapp, Int. J. Mass Spectrom. Ion Processes 40 (1981) 87.
[15] F. N. Hodgson, M. Desjardins, W. Baun, Mass Spectrom. Conference, San Francisco, paper 78 (1965) 444.
[16] D. Consalvo, A. Mele, D. Stranges, A. Giardini-Guidoni, R. Teghil, Int. J. Mass Spectrom. Ion Processes 91 (1989) 319.
[17] I. S. Ignatev, H. F. Schaeffer III, J. Chem. Phys. 103 (1995) 7025.
[18] H. Lavendy, J. M. Robbe, J. P. Flament, G. Pascoli, J. Chim. Phys. 94 (1997) 649.
[19] H. Lavendy, J. M. Robbe, J. P. Flament, G. Pascoli, J. Chim. Phys. 94 (1997) 1779.
[20] D. C. Parent, Int. J. Mass Spectrom. Ion Processes 116 (1992) 257.
[21] D. C. Parent, Int. J. Mass Spectrom. Ion Processes 138 (1994) 307.
[22] A. D. Becke, J. Chem. Phys. 84 (1986) 4524.
[23] A. D. Becke, J. Chem. Phys. 88 (1988) 2547.
[24] C. Lee, W. Yang, R. G. Parr, Phys. Rev. B, 37 (1988) 785.
[25] A. D. Becke, J. Chem. Phys. 88 (1988) 1053.
[26] A. D. Becke, J. Chem. Phys. 98 (1993) 5648.
[27] W. Kohn, L. J. Sham, Phys. Rev. A 140 (1965) 1133.
[28] R. Krishnan, J. S. Binkley, R. Seeger, J. A. Pople, J. Chem. Phys. 72 (1980) 650.
[29] M. J. Frisch, G. M. Trucks, H. B. Schlegel, P. MW. Gill, B. G. Johnson, M. A. Robb, J. R. Cheeseman, T. Keith, G. A. Petersson, J. A. Montgomery, K. Raghavachari, M. A. Al-Laham, V. G. Zakrzewski, J. V. Ortiz, J. B. Foresman, J. Ciolowski, B. B. Stefanov, A. Nanayakkara, M. Challacombe, C. Y. Peng, P. Y. Ayala, W. Chen, M. W. Wong, J. L. Andres, E. S. Replogle, R. Gomperts, R. L. Martin, D. J. Fox, J. S. Binkley, D. J. Defrees, J. Baker, J. P. Stewart, M. Headgordon, C. Gonzalez, J. A. Pople, Gaussian 94, Revision C.3, Gaussian, Inc., Pittsburgh, PA, 1995.
[30] D. W. Ewing, G. V. Pfeiffer, Chem. Phys. Lett. 134 (1987) 413.
[31l K. Raghavachari, J. Chem. Phys. 84 (1986) 5672.
[32] W. Weltner Jr, R. J. Van Zee, Chem. Rev. 89 (1989) 1713.
[33] G. Froudakis, A. D. Zdetsis, M. Mülhaüser, B. Engels, S. D. Peyerimhoff, J. Chem. Phys. 101 (1994) 6790.
[34] J. D. Presilla-Márquez, C. M. L. Rittby, W. R. M. Graham, J. Chem. Phys. 106 (1997) 8367.
[35] M. Mülhaüser, G. Froudakis, A. Zdetsis, S. D. Peyerimhoff, Chem. Phys. Lett. 204 (1993) 617.